CORE
Metadata, citation and similar papers at core.ac.uk
Provided by UNT Digital Library

Lithographic Characterization of Low-Order Aberrations in a 0.3-NA EUV Microfield Exposure Tool

Patrick Naulleau,[1] Jason Cain,[2] Kim Dean,[3] and Kenneth A. Goldberg[4]

[1] College of Nanoscale Science and Engineering, University at Albany, NY 12203
[2] EECS Department, University of California, Berkeley, CA 94720
[3] SEMATECH, Austin, TX 78741
[4] Center for X-Ray Optics, Lawrence Berkeley National Laboratory, Berkeley, CA 94720

ABSTRACT

Although tremendous progress has been made in the crucial area of fabrication of extreme ultraviolet (EUV) projection optics, the realization diffraction-limited high numerical aperture (NA) optics (above 0.2 NA) remains a concern. The highest NA EUV optics available to date are the 0.3-NA Microfield Exposure Tool (MET) optics used in an experimental exposure station at Lawrence Berkeley National Laboratory [1] and commercial METs [2] at Intel and SEMATECH-North. Even though these optics have been interferometrically demonstrated to achieve diffraction-limited wavefront quality, the question remains as to whether or not such performance levels can be maintained after installation of the optics into the exposure tool.

Printing-based quantitative aberration measurements provide a convenient mechanism for the characterization of the optic wavefront error in the actual lithography tool. We present the lithographic measurement of low-order aberrations in the Berkeley MET tool, including a quantitative measurement of astigmatism and spherical error and a qualitative measurement of coma. The lithographic results are directly compared to interferometry results obtained from the same optic. Measurements of the Berkeley MET indicate either an alignment drift or errors in the interferometry on the order of 0.5 to 1 nm.

Keywords: extreme ultraviolet, lithography, alignment, aberrations

1. INTRODUCTION

Extreme ultraviolet (EUV) lithography [1] remains the leading candidate for high-volume manufacturing of nanoelectronic devices at feature sizes of 32 nm and below. Sub-30 nm resolution microfield EUV lithography tools have recently been developed to enable the development of supporting technologies such as resists and masks. One such tool has been operational at Lawrence Berkeley National Laboratory since early 2004 [2, 3]. The Berkeley tool relies on a synchrotron as its source of EUV radiation. A programmable coherence illuminator [4] enables the nominally coherent synchrotron source [5, 6] to be used for lithography. The lithographic optic used in the Berkeley tool is a 0.3-numerical aperture (NA) Microfield Exposure Tool (MET) optic [7, 8], a centrally obscured two-element, axially symmetric 5X reduction optical system manufactured by Zeiss. The central obscuration has a radius equal to 30% of the full pupil radius, producing an annular pupil.

Operating at a wavelength of 13.5 nm, EUV lithography systems require extremely tight alignment tolerances. Optical system alignment errors manifest themselves primarily as low-order aberrations such as astigmatism, coma, and spherical error. This is especially true for smaller scale systems like the MET optic, which is comprised of only two optical elements. Printing-based quantitative aberration measurements provide a convenient mechanism for the characterization of the optic wavefront error in the actual lithography tool. Here we present the lithographic measurement of low-order aberrations in the Berkeley MET tool, including a quantitative measurement of astigmatism and spherical error and a qualitative measurement of coma.

2. MEASUREMENT METHOD

Numerous methods have been demonstrated enabling print-based quantitative aberration extraction [9–11]; however, these methods typically rely on the use of phase shift masks and/or the ability to print at the diffraction limit of the optic.

Given the current status of EUV lithography, both these restriction pose significant problems; phase-shift EUV masks are difficult to fabricate at any resolution let alone the diffraction-limited resolution often required for aberration characterization, and current resist technology is limited to resolving at approximately twice the diffraction limit of 0.3-NA EUV optics. These limitations preclude using the methods described in the literature for EUV applications at the present time.

Given that the immediate goal of the work presented here is to characterize the alignment stability of the MET optic, we can safely restrict ourselves to measuring only a small subset of the possible aberrations. Here we concentrate on astigmatism, spherical, and coma, where the first two are addressed quantitatively and the third qualitatively.

Astigmatism is readily measured by determining the relative longitudinal focal position of the optic as a function of feature orientation. Astigmatism can be fully quantified by performing this measurement on at least four different feature orientations, for example 0°, 90°, 45°, and -45°. Operating at the diffraction limit is not required for this test, although using finer resolution patterns can be helpful for improving the sensitivity to focus.

Spherical aberration can be viewed as a linear focus dependence on radial offset in the pupil. The center of the optic, for example, focuses to a different longitudinal position than does the edge of the optic. Thus, when the diffraction pattern of the object being imaged, combined with the illumination pupil fill, occupies a significant radial range in the pupil, imaging performance will suffer. If this radially-dependent focus shift can be measured lithographically, then the spherical error present in the optic can be quantified. In practice, when using large pupil fills such a measurement can be rather difficult due to the inherent averaging of the pupil characteristics over the area covered by the pupil fill. The use of small pupil fills, however, allows for isolation of small radial regions in the pupil. Furthermore, the ability to arbitrarily position the pupil fill provides for even more measurement flexibility. The programmable illuminator [4] available on the MET printing system at Berkeley [2, 3] is particularly well-suited to these tasks.

Sampling of different radial locations in the pupil can be achieved in two different ways when using a small disk-type pupil fill [12]: one way to use diffraction from the object itself to set the radial sampling and another is to move the illumination in the pupil. The problem with the former, given the central obscuration of the optic, is that with a small pupil fill the DC filtering imparted by the central obscuration causes frequency doubling requiring resist resolution capabilities down to 12 nm in order to sample out to the edge of the pupil. To overcome the resist resolution problem in the centrally-obscured case, the pupil fill can be offset in the *y* direction to just clear the obscuration (Figure 1). In this configuration, to avoid problems with obscuration of diffracted orders, only vertical lines and spaces (which diffract in the horizontal direction) should be used.

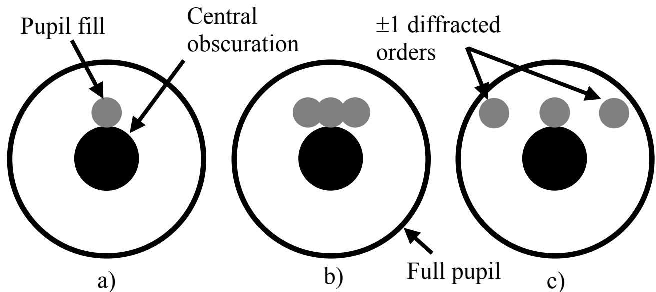

Figure 1. Configuration enabling mask diffraction to be used to sample different radial offsets while avoiding the frequency doubling problem arising in the centrally obscured MET optic. a) the pupil fill alone or in the presence of very coarse lines, b) the pupil fill modulated by the diffraction from medium-pitch lines, and c) the pupil fill modulated by the diffraction from fine-pitch lines.

In the second approach (Figure 2), we are free to use relatively coarse features and quantify the focus shift as a function of pupil fill position. To minimize edge effects from the pupil, the coarse features used to track focus are selected to diffract in a direction orthogonal to the pupil-fill offset. It is important to note that this technique relies on the use of a highly flexible pupil-fill illuminator such as the programmable scanning illuminator used in the Berkeley EUV exposure station [4]. Modeling has shown [12] these methods to provide excellent sensitivity and selectivity to spherical error.

Figure 2. Variable offset pupil fill method to sample different radial positions in the optic. Pupil fill pattern is shown modulated by a coarse horizontal line-space structure on the mask.

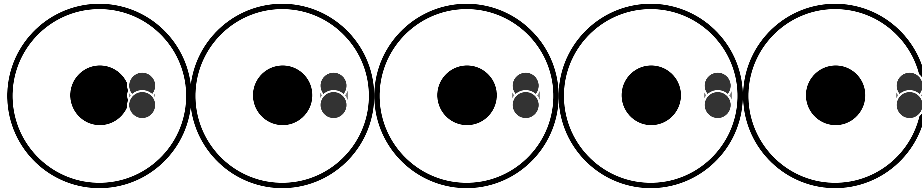

Due to EUV-specific limitations with resist resolution and difficulties in manufacturing phase-shift masks, quantitative measurement of coma error is very challenging. Here qualitatively characterize the coma by considering the orientation dependence of the process-window analysis and comparison to modeling results.

3. MEASUREMENT RESULTS

The measurement methods described above have been used to lithographically characterize the low-order aberrations in the MET optic at Berkeley. In all cases, the analyzed printed patterns were recorded in a 125-nm thick layer of Rohm and Haas *MET-1K* resist (XP3454C). Post application and exposure bake temperatures were 120° and the bake times were 60 and 90 seconds, respectively. First we present the measured astigmatism results, for more details on the measurements see Ref. [13]. Table 1 shows the measured astigmatism across the 200 × 600 µm field in a 3 × 3 grid. Both the individual astigmatism components as well as the total astigmatism are shown. The locations in the table correspond to the relative physical locations of the measured points in the printed field. Based on separate print-based focus extraction accuracy results [13] we expect the astigmatism measurement accuracy to be 0.1 nm rms.

We also directly compare the lithographic results to the interferometric results [14] obtained nearly a year earlier. Table 2 shows the cross-field interferometrically measured astigmatism data. We see significant discrepancies both in the total astigmatism magnitude and the individual astigmatism components. Errors near 0.5 nm are evident over a large portion of the field and the data shows that at some points in the field the astigmatism has actually improved over time. Despite these large changes, the field-averaged astigmatism is not greatly increased from the interferometric state: 0.31 nm for the interferometry measurement versus 0.41 for the lithographic measurement.

Table 1. Astigmatism measured lithographically at nine points in a 3 × 3 grid spanning the field of view. The reported results are rms magnitudes in nanometers. The locations in the table correspond to the relative physical locations of the measured points in the field.

0° astigmatism

-0.467	-0.434	-0.188
-0.518	-0.427	-0.036
-0.481	-0.511	-0.002

45° astigmatism

-0.003	-0.237	-0.314
-0.032	-0.079	-0.216
-0.032	-0.089	-0.160

Total astigmatism magnitude

0.468	0.494	0.365
0.519	0.433	0.219
0.482	0.518	0.160

Table 2. Astigmatism measured interferometrically at nine points in a 3 × 3 grid spanning the field of view. The reported results are rms magnitudes in nanometers. The locations in the table correspond to the relative physical locations of the measured points in the field.

0° astigmatism

-0.239	0.001	0.317
-0.355	-0.073	0.379
-0.275	-0.065	0.688

45° astigmatism

0.157	-0.035	-0.356
-0.173	-0.013	-0.160
-0.030	-0.031	0.211

Total astigmatism magnitude

0.286	0.035	0.476
0.394	0.074	0.412
0.277	0.072	0.719

Next we consider the measurement of spherical error. In all cases, the pupil fill was a disk of radius 0.15 σ. The exposure procedure for the CD-dependent focus-shift wafer is to generate a standard focus-exposure matrix. Best focus is then found for each feature size by analyzing the through-focus behavior of the printed feature size and line edge roughness (LER). To mitigate any concerns with respect to field curvature, the mask is designed such that the complete set of analyzed CDs falls within an area of approximately 10 × 10 µm out of the full 200 × 600 µm field size. For the pupil-fill-offset-dependent results, the exposure procedure is to generate a series of focus-exposure matrices on the same

wafer; each one exposed using a different pupil-fill offset. The offset is chosen to lie in the *x* direction owing to the larger available pupil-fill range. The Berkeley programmable illuminator supports up to a σ of 1.2 in *x* and only 0.8 in *y*. A total of three offsets were used: σ equal 0.475, 0.65, and 0.825, respectively. Best focus from the prints is then found for one or more feature sizes for each pupil fill offset. Focus was determined for horizontal features including half pitches of 50, 60, and 70 nm features.

Figures 3 and 4 show plots of the measured focus as a function of CD and offset, respectively. The error bars are based on the separately characterized focus measurement accuracy [12]. For the case of the offset-dependent focus shift, we must further be concerned with focus errors arising from location dependence within the array of exposed die. This is because we are now directly comparing the focus as measured in multiple columns in the in the array (each column corresponding to a different pupil offset setting), whereas for the CD case, all the focus data is extracted from a single column in the exposed matrix, thus exposure-position-dependent focus errors will be common to all CDs and need not be taken into consideration.

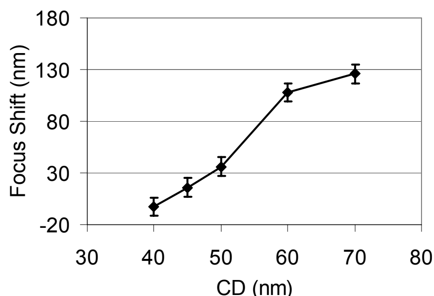

Figure 3. Measured focus as a function of feature half pitch (CD). The pupil fill was a disk of radius 0.15 σ positioned directly above the central obscuration in accordance with Figure 1.

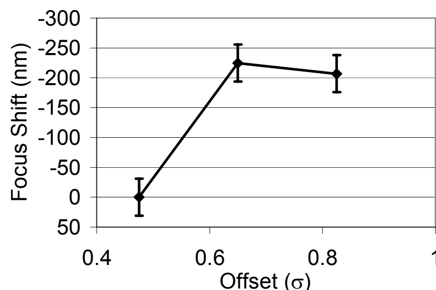

Figure 4. Measured focus as a function of pupil-fill offset. The pupil fill was a disk of radius 0.15 σ and offset in the *x* direction. A total of three offsets were used: σ equal 0.475, 0.65, and 0.825, respectively.

It is evident from the results in Figures 3 and 4 that the optic displays significant focus shift as a function of radius and thus suffers from spherical aberration. To quantify this observation, a least-squares minimization approach is used. The function we minimize is the difference between the measured focus signature and the predicted focus signature as a function of spherical error magnitude. The predicted signature is determined through PROLITH [15] modeling. Figure 5 shows the results of the minimization. The error function displays smooth behavior and a clear minimum. Minimizing the error, we find the predicted spherical aberration rms magnitude to be 1 nm as compared to the 0.1 nm rms value measured during the interferometric alignment of the optic a year earlier [14].

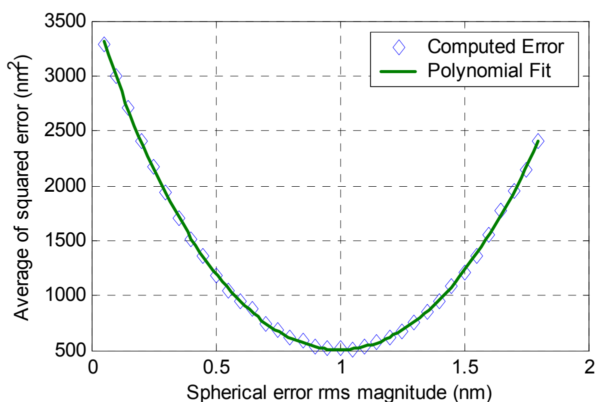

Figure 5. Least squares regression results to determine the expected value of the spherical aberration. The minimized function is the difference between the measured focus signature and the predicted focus signature as a function of spherical error magnitude. The predicted signature is determined through PROLITH modeling. Minimizing the error, yields a predicted spherical aberration rms magnitude of 1 nm.

Finally we consider the qualitative characterization of coma. Figure 6 shows the measured orientation dependence of the 50-nm equal-line-space process window. We use the same elbow pattern features as used above for the characterization of astigmatism. From these results we see a possible depth-of-focus (DOF) spread among the four different orientations of ~50 nm.

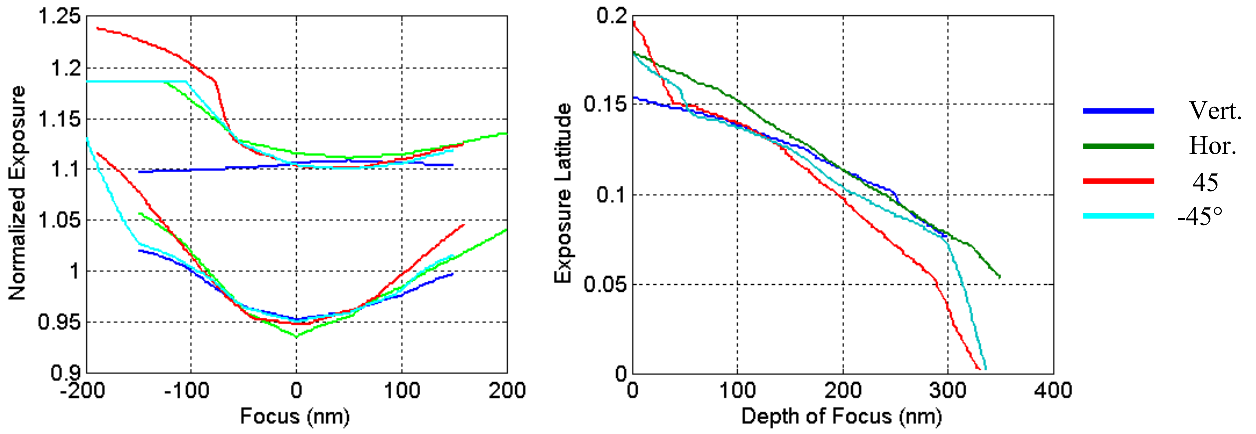

Figure 6. Lithographically-measured orientation dependence of the 50-nm equal-line-space process window.

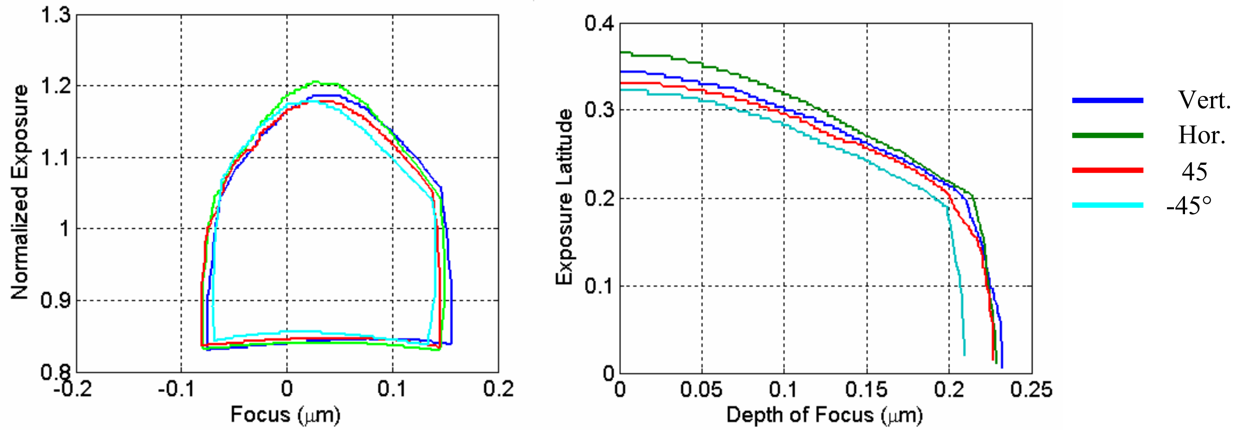

Figure 7. Predicted orientation dependence of the 50-nm equal-line-space aeriel-image process window. Assumes 0.5 nm rms of coma (the interferometrically measured value) along with the lithographically-measured astigmatism and spherical error values presented above. For the rest of the aberrations the interferometically-measured values are used.

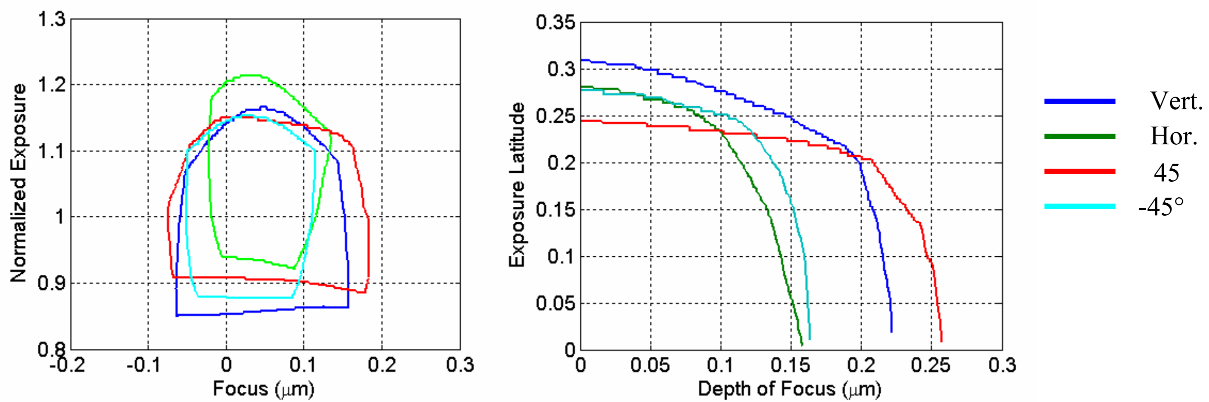

Figure 8. Predicted orientation dependence of the 50-nm equal-line-space aeriel-image process window. Assumes 1 nm rms of coma with the rest of the aberrations as in Figure 7.

To gain a qualitative understanding of the coma magnitude, we use PROLITH the compute the orientation dependence of the aerial-image-based process window. The first case we look at (Figure 7) assumes 0.5 nm rms of coma (the interferometrically measured value) along with the lithographically-measured astigmatism and spherical error values presented above. For the rest of the aberrations we also use the interferometrically-measured values. Here we see a DOF-spread of 25 nm, close to the values measured lithographically. For the next case (Figure 8) we set the coma value to 1 nm rms while keeping all the other aberrations the same. Here we significant DOF spread (~100 nm) which is clearly much worse than observed lithographically. From these results we can conclude that the coma magnitude in the actual optic should be in the 0.5–1.0 nm rms range

4. DISCUSSION

The field-dependent astigmatism in the 0.3-NA MET optic at Berkeley has been measured lithographically using an orientation-dependent focus-shift method. Reproducibility measurements have demonstrated the uncertainty in the lithographic astigmatism values to be ~0.1 nm rms. This compares favorably with the 0.06-nm precision previously demonstrated from EUV interferometry [13]. Comparisons between interferometric measurements and lithographic measurements performed nearly one year later indicate that alignment drifts have occurred affecting the astigmatism by nearly 0.5 nm rms over much of the field. Despite this large change, the field-averaged astigmatism is not greatly increased from the interferometric state: 0.31 nm for the interferometry measurement versus 0.41 for the lithographic measurement.

Moreover, pupil-position-dependent focus-shift measurements have been used to quantify the spherical aberration. These measurements were made possible by the use of a programmable coherence illuminator. A 1-nm rms spherical error has been found in the MET as compared to the 0.1-nm value expected based on interferometry a year earlier. We have no definitive explanation for this change in spherical aberration, however, it is most likely due to interferometry errors or longitudinal placement error of the object plane. Although, in principle, correctable through a 400-µm shift of the object plane, such a correction is not feasible in practice due to range limits on the image-side wafer-height sensor. To correct this error, the height sensor would have to be repositioned, a complicated task incurring significant risk.

Finally, comparisons of the orientation dependence of the process window between lithographic and modeling results shows the coma error to be in the 0.5–1 nm rms range.

ACKNOWLEDGMENTS

The authors are greatly indebted to Paul Denham and Brian Hoef of the Center for X-Ray Optics at Lawrence Berkeley National Laboratory for expert support with the exposure tool as well as the entire CXRO engineering team for bringing the exposure tool to fruition. This research was performed at Lawrence Berkeley National Laboratory and supported by SEMATECH. Lawrence Berkeley National Laboratory is operated under the auspices of the Director, Office of Science, Office of Basic Energy Science, of the US Department of Energy.

REFERENCES

1. R. Stulen and D. Sweeney, "Extreme ultraviolet lithography," IEEE J. Quantum Electron. **35**, 694-699 (1999).
2. P. Naulleau, K. Goldberg, J. Cain, E. Anderson, P. Denham, K. Jackson, S. Rekawa, F. Salmassi, G. Zhang, "EUV Microexposures at the ALS using the 0.3-NA MET Optic," J. Vac. Sci. & Technol. B **22**, 2962-2965 (2004).
3. P. Naulleau, K. Goldberg, E. Anderson, J. Cain, P. Denham, B. Hoef, K. Jackson, A. Morlens, S. Rekawa, K. Dean, "EUV microexposures at the ALS using the 0.3-NA MET projection optics," Proc. SPIE **5751** 56-63 (2005).
4. P. Naulleau, P. Denham, B. Hoef, and S. Rekawa, "A design study for synchrotron-based high-numerical-aperture scanning illuminators," Opt. Comm. **234**, 53-62 (2004).
5. D. Attwood, G. Sommargren, R. Beguiristain, K. Nguyen, J. Bokor, N. Ceglio, K. Jackson, M. Koike, and J. Underwood, "Undulator radiation for at-wavelength interferometry of optics for extreme-ultraviolet lithography," Appl. Opt. **32**, 7022-7031 (1993).
6. C. Chang, P. Naulleau, E. Anderson, and D. Attwood, "Spatial coherence characterization of undulator radiation," Opt. Comm. **182**, 24-34 (2000).

7. J. Taylor, D. Sweeney, R. Hudyma, L. Hale, T. Decker, G. Kubiak, W. Sweatt, N. Wester, “EUV Microexposure Tool (MET) for near-term development using a high NA projection system,” 2nd International EUVL Workshop October 19-20, 2000 (www.sematech.org/public/resources/litho/euvl/euvl2000/documents/707_SYS07_taylor.pdf)
8. R. Hudyma, J. Taylor, D. Sweeney, L. Hale, W. Sweatt, N. Wester, “E-D characteristics and aberration sensitivity of the Microexposure Tool (MET),” 2nd International EUVL Workshop October 19-20, 2000 (http://www.sematech.org/public/resources/litho/euvl/euvl2000/documents/hudyma.pdf).
9. P. Dirksen, C. Juffermans, R. Pellens, M. Maenhoudt, P. Debisschop, “Novel aberration monitor for optical lithography,” Proc. SPIE **3679**, 77-86 (1999).
10. H. Fukuda, K. Hayano, S. Shirai, “Determination of high-order lens aberration using phase/amplitude linear algebra,” J. Vac. Sci. & Technol. B **17**, 3318-3321 (1999).
11. G. Robins, K. Adam, A. Neureuther, “Measuring optical image aberrations with pattern and probe based targets,” J. Vac. Sci. & Technol. B **20**, 338-343 (2002).
12. P. Naulleau, J. Cain, K. Goldberg, “Lithographic characterization of the spherical error in an EUV optic using a programmable pupil fill illuminator,” Appl. Opt., *to be published* (2005).
13. P. Naulleau, J Cain, and K. Goldberg, “Lithographic characterization of the field dependent astigmatism and alignment stability of a 0.3 numerical aperture EUV microfield optic,” J. Vac. Sci. & Technol. B, *to be published* (2005).
14. K. Goldberg, P. Naulleau, P. Denham, S. Rekawa, K. Jackson, E. Anderson, J. Liddle, “At-Wavelength Alignment and Testing of the 0.3 NA MET Optic,” J. Vac. Sci. & Technol. B **22**, 2956-2961 (2004).
15. PROLITH is a registered trademark of KLA-Tencor Corporation, 160 Rio Robles, San Jose, California 95134.